MORPHOLOGY OF INSTANTANEOUS FLAME SURFACES IN LAMINAR AND TURBULENT LEAN H_2-AIR FLAMES

H. C. Lee*, P. Dai*, M. Wan* and A.N. Lipatnikov**
lipatn@chalmers.se
*Southern University of Science and Technology, Shenzhen, 518055, China
**Chalmers University of Technology, Gothenburg, 412 96, Sweden

Abstract
Direct Numerical Simulation (DNS) data obtained from two lean (the equivalence ratio $\phi = 0.5$ or 0.35) complex-chemistry hydrogen-air flames propagating in forced turbulence in a box are analysed. Karlovitz number Ka is varied from 1.2 to 6.4 or from 86 to 125 at $\phi = 0.5$ or 0.35, respectively. The focus of consideration is placed on qualitative changes in morphology of instantaneous flame surfaces with increasing rms velocity u' from zero to double laminar flame speed in the moderately lean ($\phi = 0.5$) case. DNS data obtained from unstable laminar and weakly turbulent ($Ka \leq 1.5$) flames show predominance of similar regular large-scale wrinkles of instantaneous flame surface. This observation indicates that diffusional-thermal instability dominates turbulence under such conditions. On the contrary, DNS data obtained from other explored turbulent flames show appearance of irregular small-scale wrinkles of instantaneous flame surface, but the lack of regular large-scale wrinkles associated with unstable laminar flames. This observation implies a decreasing role played by diffusional-thermal instability with increasing Ka. Since the analyzed DNS data do not show any solid sign of an important role played by the instability at $Ka > 3.5$, the data are consistent with a recently introduced criterion of importance of laminar flame instabilities in turbulent flows.

Introduction
A significant increase in turbulent burning rate with decreasing Lewis number $Le = \kappa/D$ was well documented in numerous measurements reviewed elsewhere [1,2], in recent experiments with lean hydrogen [3-5], syngas [6,7], or ammonia/hydrogen [8-10] turbulent flames, and in recent direct numerical simulation (DNS) studies of turbulent combustion of lean H_2/air [11-15] or NH_3/H_2/air [12,16] mixtures. Here, κ is molecular heat diffusivity of a mixture and D is molecular diffusivity of deficient reactant in that mixture. The phenomenon is commonly attributed to differential diffusion effects, i.e., local variations in temperature, mixture composition, and reaction rates within stretched, inherently laminar reaction zones due to imbalance of molecular fluxes of chemical energy to and heat from such zones [1,2,17-21]. While this governing physical mechanism is widely accepted and significant influence of differential diffusion effects on turbulent burning velocity U_T has been known over decades [22,23], there is no well-recognized model capable for predicting the large magnitude of an increase in U_T with decreasing Le (if Lewis number is significantly smaller than unity).

Among a few approaches put forward to accept this challenge and reviewed elsewhere [2], there is a growing interest [7,9,14,16,20,22,24,25] in a paradigm that highlights Diffusional-Thermal Instability (DTI) of laminar premixed flames characterized by $Le < Le_{cr} < 1$ [17]. While this instability is expected to be of substantial importance in weakly turbulent flames, there is no consensus on a role played by the instability at high normalized rms velocities u'/S_L or high Karlovitz numbers $Ka \propto (u'/S_L)^{3/2}(L/\delta_L)^{-1/2}$. Here, L is an integral length scale of turbulence; S_L and δ_L are laminar flame speed and thickness, respectively. This situation resembles long-term debates [1,19,26-28] on a role played by another premixed flame

instability, i.e., hydrodynamic or Darrieus-Landau (DL) one [17], in turbulent combustion. Recent DNS [29] and experimental [30,31] studies have shown that DL instability plays a substantial role in turbulent flames at low $Ka < 1$ only, in line with criteria proposed earlier by Lipatnikov and Chomiak [19] or Chaudhuri et al. [28] based on different physical reasoning.

Similarly, one could expect that DTI is of importance if Karlovitz number is less than a critical number Ka_{cr}. Such a criterion of

$$Ka < Ka_{cr} = \sqrt{15}\tau_f \omega_{\max} \tag{1}$$

has recently been obtained by Chomiak and Lipatnikov [32] by extending their previous analysis [19] of flames that are characterized by $Le \geq 1$ and, hence, are subject to DL instability only. Here, Ka is equal to a ratio of the flame time scale $\tau_f = \delta_L/S_L$ and the Kolmogorov time scale τ_K, and $\omega_{\max} = \max\{\omega(k)\}$ is the maximum growth rate of laminar-flame-surface perturbations of various wavenumbers k. Dispersion curves $\omega(k)$ obtained numerically from two-dimensional (2D) unstable lean hydrogen-air laminar flames [33,34] yield $\tau_f \omega_{\max} = O(1)$, i.e., Ka_{cr} is expected to be of unity order, but larger than unity for lean H_2-air flames [32].

Existence of a critical Karlovitz number is in line (i) with experiments [35], which showed substantially different time-dependencies of mean radii of lean H_2/air expanding spherical flames at $u' < S_L$, $u_K < S_L < u'$, and $S_L < u_K$, or (ii) with DNS data [14,36,37], which indicated that various characteristics of flame-flow interactions scaled differently in unstable laminar flames and in turbulent flames characterized by high Ka. Here, u_K is Kolmogorov velocity. Besides, by analyzing DNS data obtained from two V-shaped flames characterized by $u'/S_L = 0.72$ and 2.8, Day et al. [38, p. 1043] have stated that "with increasing turbulence levels fluctuations, at even the lowest intensity levels, appear to suppress to some extent the growth and propagation of the spherical burning cells characteristic of the thermodiffusive instability." Howarth et al. [37, p. 15] have also noted that "turbulence is beginning to dominate thermodiffusive effects" at moderate values of Ka.

The criterion given by Eq. (1) was supported by two recent target-directed DNS analyses [39,40]. Specifically, first, Lee et al. [39] simulated laminar and weakly turbulent combustion in narrow domains, with the domain width Λ being either slightly smaller or slightly larger than the neutral wavelength $\lambda_n = 2\pi/k_n$ of DTI [41-43], found using a constraint of $\omega(k > k_n) \leq 0$. Thus, DTI was enabled in the wider domain only, whereas the smoothing effect of molecular transport on flame surface overwhelmed the instability in the smaller domain [41-43]. The major idea of that DNS study goes back to the work by Matalon et al. [29,44] who proposed such a simple method to explore a role played by DL instability of laminar flames in turbulent burning. Results reported in Ref. [39] show that an increase in u'/S_L affects the flames in the two domains differently when $Ka < Ka^*$, but similarly when $Ka > Ka^*$. This finding indicates that laminar flame instabilities (enabled in the wider domain only) do not appear at Ka> 〖Ka 〗 $Ka > Ka^*$, with Ka^* being close to Ka_{cr} yielded by Eq. (1) under conditions of that study.

Second, Lipatnikov et al. [40] continued their previous DNSs [45,46] of lean H_2/air flames in forced turbulence by switching of the forcing at different instants. Due to the turbulence decay, DTI was supposed to appear at sufficiently low Ka. Analyses of flame-surface images sampled at different instants did show appearance of regular large-scale perturbations (characteristic of the instability) during the turbulence decay, with the numbers Ka associated with that transition agreeing with Ka_{cr} in Eq. (1) within an order of magnitude.

Due to importance of the discussed issue (a large increase in U_T/S_L with decreasing Le and contribution of DTI to this effect), the two aforementioned tests [39,40] of Eq. (1) are not sufficient and further research into the issue is required. Accordingly, the present work aims at exploring a role played by DTI in turbulent combustion by analyzing instantaneous flame-

surface images generated in newly designed target-directed simulations that differ substantially from the previous ones [39,40]. These new DNS cases are described in the next section. Results are presented and discussed in the third section followed by conclusions.

DNS Attributes and Diagnostic Methods

Since the present simulations are similar (with the exception of conditions) to earlier DNSs discussed in Refs. [13,39,40,45-51], only a brief summary of the used numerical tools follows.

Unsteady three-dimensional (3D) DNSs of statistically one-dimensional and planar, lean H_2-air flames propagating in forced turbulence in a box under room conditions were performed using a chemical mechanism (9 species and 22 reversible reactions) by Kéromnès et al. [52], with mixture-averaged molecular transport and chemical reaction rates being modeled using open-source library *Cantera*-2.3 [53]. Navier-Stokes, energy, and species transport equations written in the low-Mach-number formulation were integrated using solver *DINO* [54].

A rectangular computational domain of $\beta\Lambda \times \Lambda \times \Lambda$ was discretized using a uniform Cartesian grid of $\beta N \times N \times N$ cells (the values of Λ, β, and N will be reported later). The adopted numerical meshes ensure more than 20 grid points across the thickness δ_L in low Le cases. Along the streamwise direction x, inflow and outflow boundary conditions were set. Other boundary conditions were periodic. Turbulence was generated using a variable-density modification [55] of the linear velocity forcing method within a rectangular domain of $0.5\Lambda \leq x \leq 8\Lambda$, with the turbulence evolution being simulated for at least 50 integral time scales $\tau_t = L/u'$. This method yields $L = u'^3/\varepsilon_0 \approx 0.19\Lambda$ [45], where $\varepsilon_0 = 2\nu\langle S_{ij}S_{ij}\rangle$ is dissipation rate averaged over forced turbulence volume; $S_{ij} = 0.5\left(\partial u_i/\partial x_j + \partial u_j/\partial x_i\right)$ is the rate-of-strain tensor, and the summation convention applies to repeated indexes.

Combustion simulations were started by embedding a steady planar laminar flame solution obtained using *Cantera*-2.3 [53] at $x = \beta\Lambda/2$. Subsequently, the simulations were run for at least $30\tau_t$. To keep the flame within the forced-flow domain, the mean inlet velocity was manually changed when necessary.

Table 1. Characteristics of laminar flames.

ϕ	Le	S_L, m/s	δ_L^T, mm	Ka_{cr}	λ_n, mm
0.35	0.36	0.12	0.92	7.7	2.7
0.43	1.0	0.58	0.31	-	-
0.50	0.39	0.58	0.41	4.3	1.3

Characteristics of the aforementioned steady planar laminar premixed flames for the studied mixtures are reported in Table 1. Here, ϕ is the equivalence ratio; $\delta_L = (T_b - T_u)/\max|\nabla T|$; subscripts u and b refer to unburned and burned gases, respectively; and T is the temperature. These characteristics have been computed using the same chemical mechanism [52] and open-source library *Cantera*-2.3 [5]. The quantities Ka_{cr} and λ_n will be discussed later.

The simulation conditions are summarized in Table 2, where $Da = \tau_t/\tau_f$ is Damköhler number; the Reynolds number $Re_\lambda = u'\lambda/\nu_u$ and Karlovitz number $Ka = \tau_f/\tau_K$ are evaluated using Taylor length scale $\lambda = u'\left(15\nu_u/\overline{\langle\varepsilon\rangle}_{le}\right)^{1/2}$ and Kolmogorov time scale $\tau_K = \left(\nu_u/\overline{\langle\varepsilon\rangle}_{le}\right)^{1/2}$, respectively; the dissipation rate $\overline{\langle\varepsilon\rangle}_{le}$ is averaged over flame-brush leading zone characterized by $0.01 < \langle c_F\rangle(x,t) < 0.05$; $c_F = 1 - Y_F/Y_{F,u}$ designates combustion progress variable defined using the fuel mass fraction Y_F , with $\langle c_F\rangle$ being its transverse-averaged value; $\eta_K = \left(\nu_u^3/\overline{\langle\varepsilon\rangle}_{le}\right)^{1/4}$ is Kolmogorov length scale; and $\Delta x = \Lambda/N$ is the grid spacing.

Table 2. DNS conditions.

Case	ϕ	Le	$\frac{u'}{S_L}$	$\frac{L}{\delta_L^T}$	Re_λ	Ka	Da	$\frac{\Delta x}{L}$	$\frac{\Delta x}{\eta_K}$	N	β	Λ, mm
LF025	0.5	0.39	0.25	2.6	4.9	1.2	10.4	0.02	0.10	256	12	5.6
LF05	0.5	0.39	0.5	2.6	10.0	1.5	5.2	0.02	0.17	256	12	5.6
LF10	0.5	0.39	1.0	2.6	22.0	2.1	2.6	0.02	0.29	256	12	5.6
LF15	0.5	0.39	1.5	2.6	27.0	3.9	1.8	0.02	0.39	256	12	5.6
LF20	0.5	0.39	2.0	2.6	28.1	6.4	1.3	0.02	0.51	256	12	5.6
LF20/1	0.43	1.0	2.0	3.4	28.1	4.9	1.5	0.02	0.51	256	12	5.6
E	0.35	0.36	11.2	0.5	20	125.	0.04	0.08	1.1	64	16	2.4
F	0.35	0.36	11.2	1.2	29	85.7	0.10	0.04	1.1	128	16	5.6

The five cases LF025, LF05, LF10, LF15, and LF20 have been designed to assess the criterion given by Eq. (1) in a wider computational domain ($\Lambda = 5.6$ mm) when compared to all previously simulated moderately lean ($\phi = 0.5$) flames [20-28]. Accordingly, in these flame names, letters L and F refer to "larger flames" and numbers show u'/S_L. Flame LF20/1 is an equidiffusive counterpart of flame LF20, with ϕ being decreased to retain the same S_L.

In addition, to the newly designed larger-scale moderately lean flames, two leaner flames E and F studied by us earlier [13,48-51] are further explored here from another perspective. The point is that results plotted in Fig. 1b in the next section show that DTI is enabled in wider computational domain (case F), with perturbations with the maximum growth rate developing in that domain. On the contrary, DTI is not enabled in case E, because the domain width Λ was occasionally set too small in that case, i.e., $\Lambda < \lambda_n$. Nevertheless, U_T/S_L is significantly increased by differential diffusion effects not only in flame F but also in flame E [13].

The fact that $\Lambda < \lambda_n$ in case E was revealed by simulating unsteady 2D and 3D unstable laminar flames. Those simulations were performed using the same chemical mechanism [52], the same transport model, and the same solver DINO [53]. To trigger instability of an initially planar laminar flame, a weak sinusoidal perturbation of the axial inlet velocity with a wavenumber k was imposed at $t = 0$. Subsequently, evolution of the burning velocity

$$U_L(t) = \frac{1}{(\rho Y_F)_u \Lambda^{n-1}} \iiint |\dot{\omega}_F(\mathbf{x}, t)| d\mathbf{x} \tag{15}$$

was computed. Here, ρ is the density; $\dot{\omega}_{\mathrm{H}_2}(\mathbf{x}, t)$ is Fuel Consumption Rate (FCR); $n = 2$ or 3 in 2D or 3D case, respectively; and integration is performed over the entire domain.

Results and Discussion

Figures 1a and 1b show typical evolution of the normalized burning velocity $U_L(t)/S_L$ and the dispersion relations $\omega(k)$, respectively. The dispersion relations have been calculated by setting $k = 2\pi/\Lambda$, varying the domain width Λ, and fitting the obtained $U_L(t)/S_L$-curves with an equation of $\ln[U_L(t)/S_L - 1] \propto 2\omega t$, which results from the flame instability theory [56]. Very similar dispersion relations were earlier obtained from 2D unstable lean hydrogen-air complex-chemistry laminar flames by other research groups, e.g., see Refs. [33,34]. It is worth stressing that the growth rate ω vanishes at the neutral wavenumber k_n and, i.e., perturbations decay if $k > k_n$. Stability of laminar flames to small-scale perturbations was earlier predicted by various theories [41-43] and is attributed to dampening such perturbations by molecular transport. Accordingly, perturbations with length scales $\lambda < \lambda_n = 2\pi/k_n$ observed in images of turbulent flame surfaces, discussed later, are hardly associated with intrinsic laminar flame instabilities.

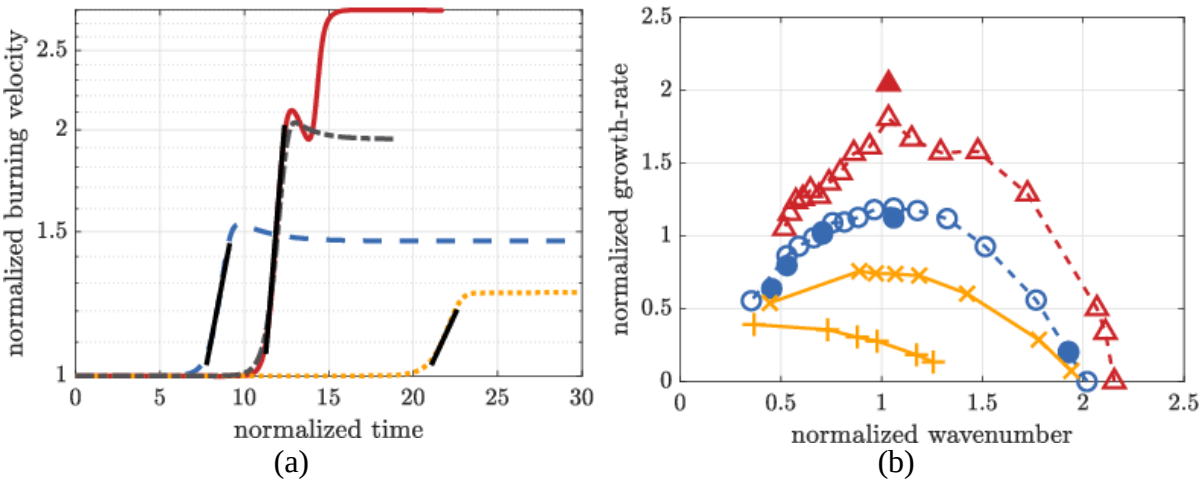

Figure 1. (a) Evolution of normalized burning velocity $U_L(t)/S_L$ computed for $k = 2\pi/\Lambda$. Red solid or blue dashed line shows 2D results computed at $\phi = 0.35$ and $\Lambda = 5.6$ mm or $\phi = 0.5$ and $\Lambda = 2.4$ mm, respectively. Black dotted-dashed line shows 3D results obtained at $\phi = 0.5$ and $\Lambda = 2.4$ mm mm. Black solid straight lines show fits to the $U_L(t)/S_L$-curves, used to calculate instability growth rates. Time is normalized using τ_f. (b) Dispersion relations obtained at $\phi = 0.35$ (red triangles) or $\phi = 0.35$ (blue circles). 3D results are plotted in filled symbols, with open symbols showing 2D results. Gtowth rate and wavenumber are normalized using τ_f and δ_L, respectively.

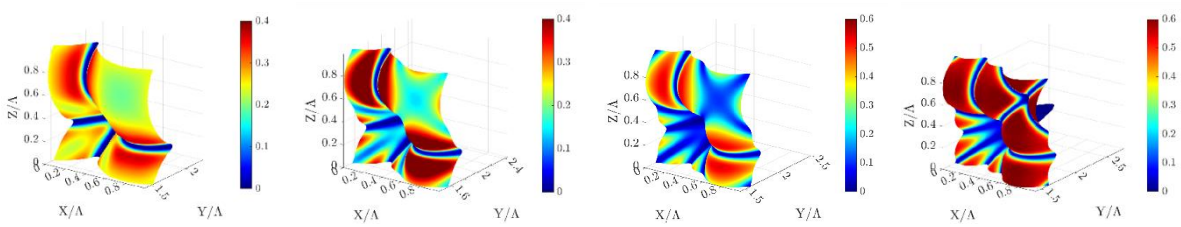

(a) (b) (c) (d)

Figure 2. Images of the instantaneous iso-surfaces $c_F(\mathbf{x}, t) = 0.5$, with color bars showing the local FCR $\dot{\omega}_{\mathrm{H}_2}(\mathbf{x}, t)$ normalized with the maximum rate $\dot{\omega}_{\mathrm{H}_2,L}^{\max}$ obtained from the unperturbed laminar flame. Unstable laminar flame, $\phi = 0.5$, $\Lambda = 5.6$ mm, initial sinusoidal perturbation with wavenumber $k = 2\pi/\Lambda$.
(a) $t/\tau_f = 12.4$, (b) $t/\tau_f = 14.1$, (c) $t/\tau_f = 14.5$, (d) $t/\tau_f = 17.2$.

Comparison of open and filled symbols in Fig. 1b indicates that the growth rates computed in 2D and 3D cases are close to one another, in line with earlier simulations with single-step chemistry [57] and complex chemistry [58]. The normalized neutral wavenumbers $\delta_L k_n$ are also almost the same in 2D and 3D cases. However, the burning velocity U_L is larger in 3D case, cf. curves plotted in blue dashed and black dotted-dashed lines in Fig. 1a. Values of $Ka_{cr,2}$ evaluated using the computed maximum growth rates and neutral wavelengths λ_n are reported in the two last columns, respectively, in Table 1.

Figure 2 reports images of unstable laminar flame surfaces of $c_F(\mathbf{x}, t) = 0.5$ in a moderately lean case of $\phi = 0.5$. Initially, the large-scale inlet perturbation predominates, see Fig. 2a. Subsequently, perturbations with a smaller wavelength appear, see Fig. 2c, because the growth rate $\omega(k)$ peaks at $\lambda \approx 2.4$ mm or $\lambda \approx 0.4\Lambda$ in the studied case, see blue circles in Fig. 1b. During a quasi-steady stage of the instability development, characterized by almost constant

$U_L(t) \approx 2S_L$, see curve plotted in black dotted-dashed line in Fig. 1a, the latter (smaller) perturbations predominate, see Fig. 2d.

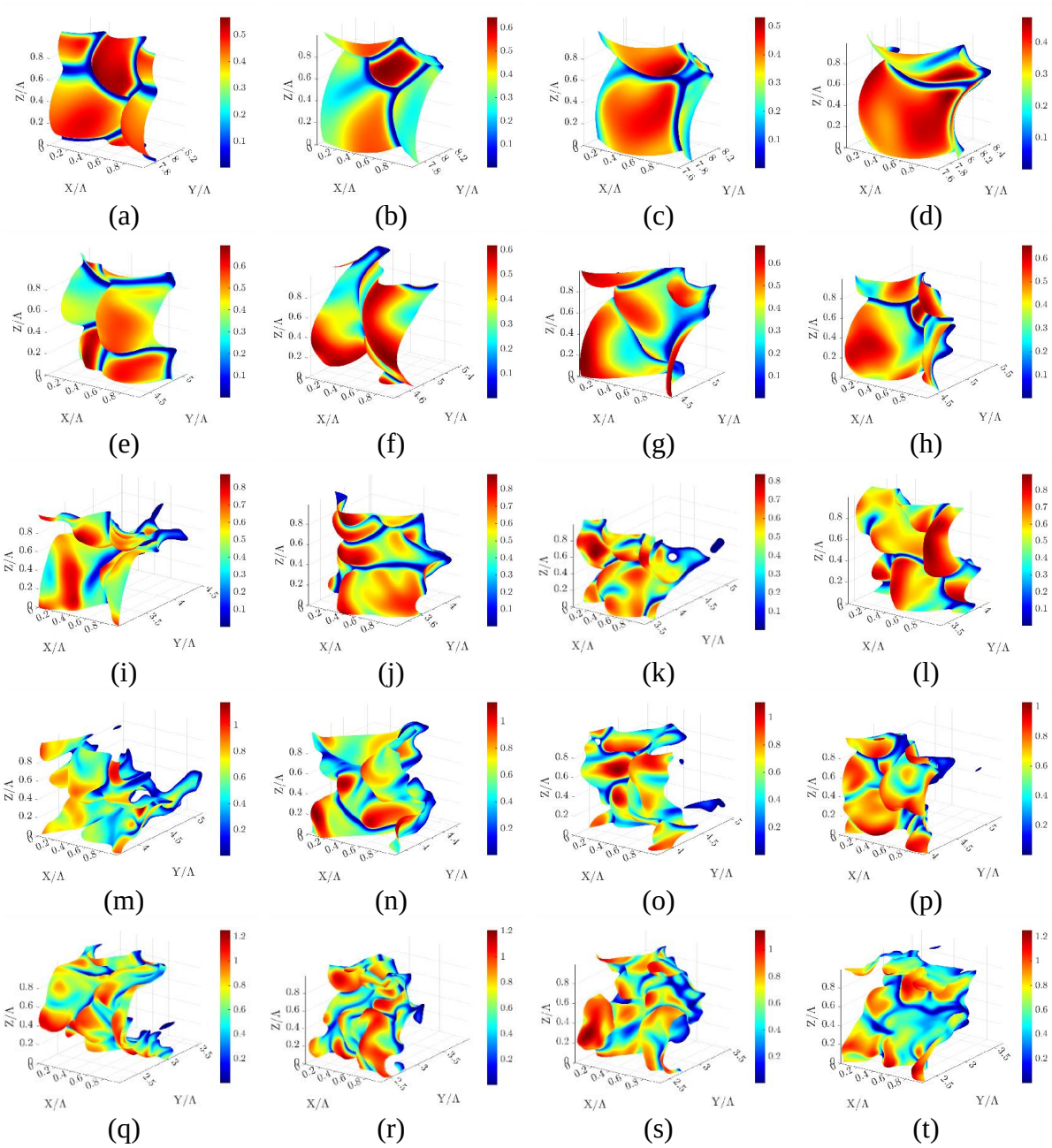

Figure 3. Images of the instantaneous iso-surfaces $c_F(\mathbf{x}, t) = 0.5$. (a)-(d) flame LF05, $t/\tau_f = 4.1$, 6.3, 8.0, and 9.4, respectively, (e)-(h) flame LF05, $t/\tau_f = 8.1$, 10.0, 12.8, and 15.4, respectively, (i)-(l) flame LF10, $t/\tau_f = 11.0$, 13.1, 15.7, and 17.1, respectively, (m)-(p) flame LF15, $t/\tau_f = 7.7$, 9.6, 11.5, and 13.4, respectively, (q)-(t) flame LF20, $t/\tau_f = 3.7$, 5.5, 7.3, and 9.5, respectively.

Colour scales in Figs. 2a and 2d show that $\dot{\omega}_{\mathrm{H}_2}[c_F(\mathbf{x}, t) = 0.5\,]$ is smaller than $\dot{\omega}_{\mathrm{H}_2,L}^{\max} \equiv \max\{\dot{\omega}_{\mathrm{H}_2,L}(c_F)\}$ reached at $c_F = 0.87$ in the unperturbed (steady, planar, and one-dimensional) laminar flame. Nevertheless, in the unstable flame, $\dot{\omega}_{\mathrm{H}_2}[c_F(\mathbf{x}, t) = 0.5\,]$ can be much larger than $\dot{\omega}_{\mathrm{H}_2,L}(c_F = 0.5) = 0.05\dot{\omega}_{\mathrm{H}_2,L}^{\max}$ in the unperturbed flame.

Figures 3a-3d and 3e-3h show representative flame-surface images in weakly turbulent cases LF025 and LF05, respectively. Sometimes, e.g., see Figs. 3a, 3b, 3e, or 3h, the surface shapes resemble the shape of quasi-steady surfaces of the unstable laminar flame, see Fig. 2d. Sometimes, e.g., see Figs. 3c, 3d, 3f, or 3g, wrinkles of the turbulent-flame surfaces are larger, but comparable with large-scale wrinkles of laminar flame surfaces during the instability growth, see Fig. 2a. In all these cases, only large-scale wrinkles (larger than the neutral wavelength $\lambda_n \approx \Lambda/4$, see blue circles in Fig. 1b) appear on the turbulent flame surface. The lack of smaller wrinkles should not be attributed to the lack of small-scale turbulent eddies, because $\eta_K = 0.3\delta_L^T = 0.02\Lambda$ in case LF05. Small-scale wrinkles seem to be smoothed out by molecular transport processes, which also known (i) to suppress small-scale perturbations of a laminar flame surface if the perturbation length scale is smaller than λ_n and, hence, (ii) to control the neutral wavelength λ_n [41-43]. In cases LF025 and LF05, turbulence is too weak and cannot overwhelm such a smoothing effect. Since even weakly turbulent flames LF025 and LF05 are characterized by a small Kolmogorov length scale $\eta_K \ll \Lambda$, the lack of small-scale wrinkles of these flame surfaces, see Figs. 3a-3d and 3e-3h, respectively, implies that DTI predominates in both cases. Such an interpretation of these DNS results is also supported by apparently narrow ranges of length scales of flame-surface perturbations in Figs. 3a-3h.

In case LF10, flame-surface images sometimes, e.g., see Figs. 3j and 3l, look like images of unstable laminar flame surfaces, see Figs. 2a-2d, or weakly turbulent flame surfaces, see Figs. 3a-3h. Specifically, there are sufficiently regular large-scale perturbations only, but small-scale wrinkles of the flame surface are hardly observed. However, at other instants, see Figs. 3i and 3k, flame-surface images are substantially different. Specifically, perturbations are less regular, and small-scale wrinkles are well pronounced.

Images of flames LF15 and LF20, shown in Figs. 3m-3p and 3q-3t, respectively, differ substantially from all images of the unstable laminar flame, see Figs. 2a-2d, or flames LF025 and LF05, see Figs. 3a-3h. Specifically, in cases LF15 and LF20, both small-scale and large-scale wrinkles are clearly visible, but the latter wrinkles are not regular, contrary to large-scale wrinkles in Figs. 2a-2d or 3a-3h. Such irregular, large-scale wrinkles are not necessarily caused by DTI but could also be attributed to large-scale turbulent eddies. Indeed, Figs. 4a and 4c show that large-scale wrinkles can predominate on the surface of equidiffusive flame LF20/1, whereas small-scale wrinkles predominate at other instants, see Figs. 4b and 4d. The major difference between images of low Le flame LF20 and equidiffusive flame LF20/1, cf. Figs. 3q-3t and 4a-4d, respectively, consists of variations in $\dot{\omega}_{\mathrm{H}_2}(\mathbf{x}, t)$ due to differential diffusion effects in the former case, whereas the flame-surface morphologies appear to be similar in both cases.

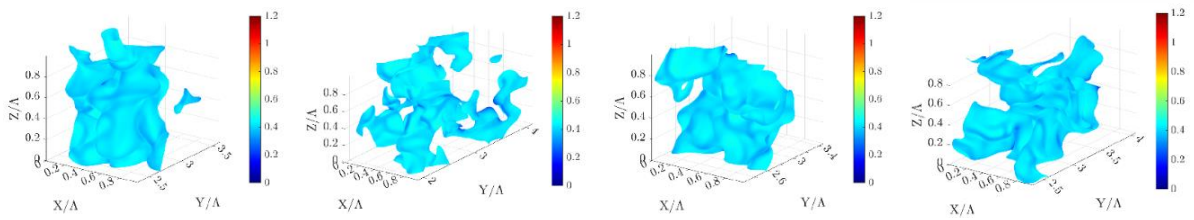

(a) (b) (c) (d)

Figure 4. Images of the instantaneous iso-surfaces $c_F(\mathbf{x}, t) = 0.5$ in equidiffusive flame LF20/1. (a) $t/\tau_f = 17.8$, (b) $t/\tau_f = 24.4$, (c) $t/\tau_f = 34.1$, (d) $t/\tau_f = 76.6$.

The flame images considered all together imply the following physical scenario. In weakly turbulent flames LF025 and LF05 ($Ka \leq 1.5$), DTI dominates turbulence. In flame LF10 ($Ka = 2.1$), both DTI and turbulence play an important role. However, flame-surface images generated in cases LF15 ($Ka = 3.9$) and LF20 ($Ka = 6.4$) do not show regular large-scale wrinkles

characteristic of the instability, maybe, with the exception of Fig. 3p. Since $Ka_{cr} = 4.3$ for the studied mixture, see Table 1, these results are consistent with the criterion given by Eq. (1), at least within the order of magnitude. Thus, the analysed DNS images indirectly support the criterion given by Eq. (1) by exploring a set of cases that differ substantially from cases addressed in the previous DNS studies of the same criterion [39,40]. Recall that the condition of $Ka = Ka_{cr}$ is crossed by (i) varying u', (ii) using a sufficiently wide (for 3D complex-chemistry DNS) computational domain, and (iii) forcing turbulence in the new cases LF025-LF20, whereas, to assess Eq. (1), Lee et al. [39] varied the width Λ, which was rather small, whereas Lipatnikov et al. [40] explored decaying turbulence in the case of a moderate Λ.

The following feature is also worth noting. The present analyses do not show an abrupt transition between two burning regimes at $Ka = Ka_{cr}$, i.e., (i) DTI-dominated regime ($Ka < Ka_{cr}$), where small-scale wrinkles do not appear on flame surface, and (ii) turbulence-dominated regime ($Ka > Ka_{cr}$), where regular large-scale wrinkles characteristic of DTI are blurred. Results obtained from flame LF10 ($Ka = 2.1$ and $Ka_{cr} = 4.3$) imply that the two regimes may alternate. For instance, Figs. 3i and 3k (or 3j and 3l) are associated with the latter (former, respectively) regime.

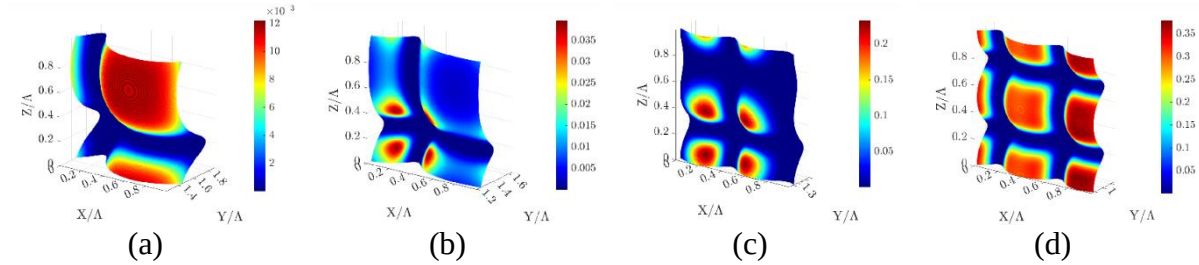

Figure 5. Images of the instantaneous iso-surfaces $c_F(\mathbf{x}, t) = 0.5$ in an unstable laminar flame,.$\phi = 0.35$, $\Lambda = 5.6$ mm, initial sinusoidal perturbation with wavenumber $k = 2\pi/\Lambda$. (a) $t/\tau_f = 5.1$, (b) $t/\tau_f = 6.0$, (c) $t/\tau_f = 6.7$, (d) $t/\tau_f = 8.0$.

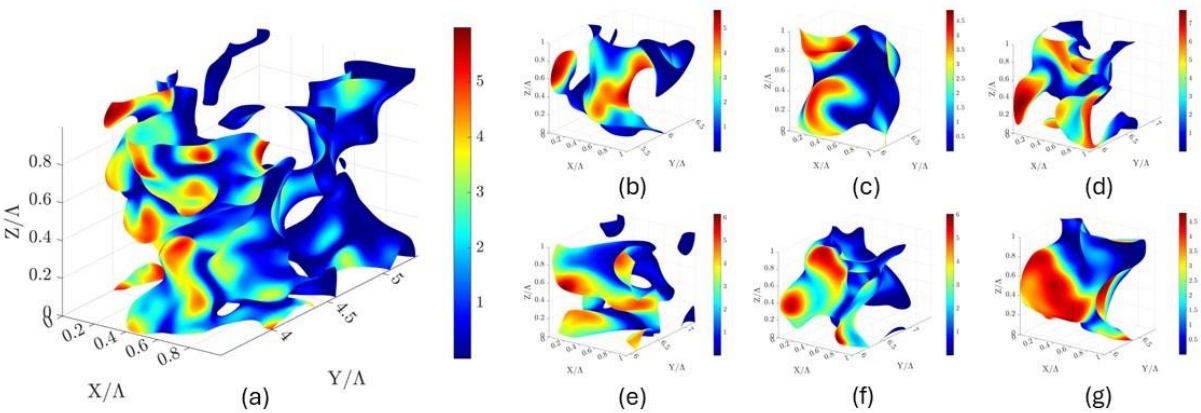

Figure 6. Images of the instantaneous iso-surfaces $c_F(\mathbf{x}, t) = 0.5$ in (a) flame F at $t/\tau_f = 23.0$ and flame E at (b) $t/\tau_f = 7.5$, (c) $t/\tau_f = 28.0$, (d) $t/\tau_f = 34.9$, (e) $t/\tau_f = 40.6$, (f) $t/\tau_f = 46.2$, (g) $t/\tau_f = 47.4$. Colour bars show the local FCR $\dot{\omega}_{\mathrm{H}_2}(\mathbf{x}, t)$ normalized with the maximum rate $\dot{\omega}_{\mathrm{H}_2,L}^{\max}$ obtained from the unperturbed laminar flame.

Images of leaner ($\phi = 0.35$) laminar and turbulent flames, see Figs. 5 and 6, respectively, are consistent with the above discussion of the interplay between DTI and turbulence. Specifically, in the laminar flame, the inlet large-scale perturbation predominates initially, see

Fig. 5a, but a smaller length scale associated with the peak growth rate, see red triangles in Fig. 1b, predominates at a later nonlinear stage of the instability development, see Fig. 5d. In both stages and during transition between them, see Figs. 5b and 5c, the range of length scales of flame surface perturbations is narrow. There are no perturbations whose length scale is about δ_L or less. Moreover, the laminar-flame-surface perturbations look regular.

On the contrary, small-scale irregular perturbations predominate in turbulent flames F and E (note that $\Lambda/\delta_L^T = 5.9$ and 2.6 in these two cases, respectively, see Table 1). While the domain width Λ is larger and smaller than the neutral wavelength λ_n in cases F and E, respectively, both flame surfaces show similar morphology, cf. Figs. 6a and 6b-6g and note that the image sizes are set different with a ratio of 56/24, because $\Lambda = 5.6$ and 2.4 mm in cases F and E, respectively. Regular, apparently large-scale perturbations, which might be associated with DTI, are only observed in Figs. 6c and 6g, but their scale is smaller than λ_n, because $\Lambda < \lambda_n$ in case E. While these images are not claimed to prove a minor role played by DTI in flame F characterized by $Ka \gg Ka_{cr}$, the images are fully consistent with such a hypothesis.

Finally, colour scales in Figs. 2c-2d and 3a-3h show that the peak local FCRs $\dot{\omega}_{\mathrm{H}_2,L}^{\max} \equiv \max\{\dot{\omega}_{\mathrm{H}_2}[c_F(\mathbf{x},t) = 0.5]\}$ are close to each other in the unstable laminar flame and weakly turbulent flames LF025 and LF05, in line with the previous discussion of importance of DTI under such conditions. Note that FCR is normalized using the same $\dot{\omega}_{\mathrm{H}_2,L}^{\max}$ in all these images of laminar and turbulent flame surfaces. Colour scales in Figs. 3m-3t indicate that $\max\{\dot{\omega}_{\mathrm{H}_2}[c_F(\mathbf{x},t) = 0.5]\}$ in turbulent flame LF15 or LF20 is significantly higher than in the unstable laminar flame, thus implying that knowledge of FCR in the latter flame is not sufficient to predict maximum local burning rate in turbulent flames characterized by a sufficiently high Ka. Comparison of colour scales in Figs. 5 and 6 also show significant difference in $\max\{\dot{\omega}_{\mathrm{H}_2,L}[c_F(\mathbf{x},t) = 0.5]\}$ and $\max\{\dot{\omega}_{\mathrm{H}_2}[c_F(\mathbf{x},t) = 0.5]\}$ in unstable laminar and turbulent flames. This large difference casts doubts on the utility of the former (laminar) quantity for modelling the influence of differential diffusion on burning rate in turbulent flows.

Conclusions

DNS data obtained from weakly turbulent flames ($u'/S_L \leq 1$ and $Ka \leq 1.5$) show predominance of regular large-scale wrinkles of instantaneous flame surface. Moreover, the amplitudes of local perturbations of fuel consumption rate in these turbulent flames and unstable laminar flames are close to each other. These findings imply that DTI dominates turbulence under such conditions.

DNS data obtained from other explored turbulent flames show appearance of irregular small-scale wrinkles of instantaneous flame surface, but the lack of regular large-scale wrinkles, which are often considered to be characteristic features of unstable flames. Moreover, the amplitudes of local perturbations of fuel consumption rate in these turbulent flames are significantly higher than the counterpart amplitudes in unstable laminar flames. These trends are more pronounced at a higher u'/S_L and Ka. These results are consistent with a hypothesis that a role played by DTI in turbulent flames is decreased with increasing Ka. Moreover, the significant differences in the aforementioned amplitudes cast serious doubts on the utility of results obtained from unstable laminar flames for developing an advanced high-fidelity model of premixed combustion in intense turbulence.

Since the analyzed DNS data do not show any solid sign of an important role played by DTI at $Ka > 3.5$, the data are consistent with the criterion given by Eq. (1).

Finally, DNS data obtained from flame LF10 imply that transition from DTI-dominated to turbulence-dominated regime of premixed combustion is not abrupt and the two regimes can coexist or/and alter in the same flame.

References

[1] Kuznetsov, V.R., Sabel'nikov, V.A., *Turbulence and Combustion*, Hemisphere, 1990.

[2] Lipatnikov, A., *Fundamentals of Premixed Turbulent Combustion*, CRC Press, 2012.

[3] Yang, S., Saha, A., Liang, W., Wu, F., Law, C.K., "Extreme role of preferential diffusion in turbulent flame propagation", *Combust. Flame* 188: 498-504 (2018).

[4] Lipatnikov, A.N., Chen, Y.-R., Shy, S.S., "An experimental study of the influence of Lewis number on turbulent flame speed at different pressures", *Proc. Combust. Inst*. 39: 2339-2347 (2023).

[5] Hsieh, H.-Y., Mousavi, S.M., Lipatnikov, A.N., Shy, S.S., "Experimental study of the influence of Lewis number, laminar flame thickness, temperature, and pressure on turbulent flame speed using hydrogen and methane fuels", *Proc. Combust. Inst*. 40: 105752 (2024).

[6] Venkateswaran, P., Marshall, A., Shin, D.H., Noble, D., Seitzman, J., Lieuwen, T., "Measurements and analysis of turbulent consumption speeds of H_2/CO mixtures", *Combust. Flame* 158: 1602-1614 (2011).

[7] Zhang, M., Wang, J., Huang, Z. "Turbulent flame structure characteristics of hydrogen enriched natural gas with CO_2 dilution", *Int. J. Hydrog. Energy* 45: 20426-20435 (2020).

[8] Lhuillier, C., Brequigny, P., Contino, F., Mounaïm-Rousselle, C., "Experimental investigation on ammonia combustion behavior in a spark-ignition engine by means of laminar and turbulent expanding flames", *Proc. Combust. Inst*. 38: 5859-5868 (2021).

[9] Wang, S., Elbaz, A.M., Arab, O.Z., Roberts, W.L., "Turbulent flame speed measurement of NH_3/H_2/air and CH_4/air flames and a numerical case study of NO emission in a constant volume combustion chamber (C.V.C.C.)", *Fuel* 332: 126152 (2023).

[10] Cai, X., Fan, Q., Bai, X.-S., Wang, J., Zhang, M., Huang, Z., Alden, M., Li, Z., "Turbulent burning velocity and its related statistics of ammonia-hydrogen-air jet flames at high Karlovitz number: Effect of differential diffusion", *Proc. Combust. Inst*. 39: 4215-4226 (2023).

[11] Aspden, A.J., Day, M.S., Bell, J.B., "Towards the distributed burning regime in turbulent premixed flames", *J. Fluid Mech*. 871: 1-21 (2019).

[12] Rieth, M., Gruber, A., Williams, F.A., Chen, J.H., "Enhanced burning rates in hydrogen-enriched turbulent premixed flames by diffusion of molecular and atomic hydrogen", *Combust. Flame* 239: 111740 (2022).

[13] Lee, H.C., Dai, P., Wan, M., Lipatnikov, A.N. "Lewis number and preferential diffusion effects in lean hydrogen-air highly turbulent flames", *Phys. Fluids* 34: 035131 (2022).

[14] Berger, L., Attili, A., Pitsch, H., "Synergistic interactions of thermodiffusive instabilities and turbulence in lean hydrogen flames", *Combust. Flame* 244: 112254 (2022).

[15] Rieth, M., Gruber, A., Chen, J.H. "The effect of pressure on lean premixed hydrogen-air flames", *Combust. Flame* 250: 112514 (2023).

[16] Coulon, V., Gaucherand, J., Xing, V., Laera, D., Lapeyre, C., Poinsot, T., "Direct numerical simulations of methane, ammonia-hydrogen and hydrogen turbulent premixed flames", *Combust. Flame* 256: 112933 (2023).

[17] Zel'dovich, Ya.B., Barenblatt, G.I., Librovich, V.B., Makhviladze, G.M., *The Mathematical Theory of Combustion and Explosions*, Consultants Bureau, 1985.

[18] Bradley, D., Lau, A.K.C., Lawes, M., "Flame stretch rate as a determinant of turbulent burning velocity", *Phil. Trans. R. Soc. London A* 338: 359-387 (1992).

[19] Lipatnikov, A.N., Chomiak, J., "Molecular transport effects on turbulent flame propagation and structure", *Prog. Energy Combust. Sci*. 31: 1-73 (2005).

[20] Hochgreb, S. "How fast can we burn, 2.0?", *Proc. Combust. Inst*. 39: 2077-2105 (2023).

[21] Pitsch, H., “The transition to sustainable combustion: Hydrogen- and carbon-based future fuels and methods for dealing with their challenges”, *Proc. Combust. Inst*. 40: 105638 (2024).
[22] Wohl, K., Shore, L., von Rosenberg, H., Weil, C.W., “The burning velocity of turbulent flames”, *Proc. Combust. I*nst. 4: 620-635 (1953).
[23] Karpov, V.P., Sokolik, A.S., “Inflammation limits in turbulized gas mixtures”, *Dokl. Akad. Nauk SSSR* 141: 393-396 (1961).
[24] Chakraborty, N., Cant, R.S., “Effects of Lewis number on flame surface density transport in turbulent premixed combustion”, Combust. Flame 158: 1768-1787 (2011).
[25] Aspden, A.J., Day, M.S., Bell, J.B., “Turbulence-flame interactions in lean premixed hydrogen: transition to the distributed burning regime”, *J. Fluid Mech*. 680: 287-320 (2011).
[26] Kobayashi, H., Tamura, T., Maruta, K., Niioka, T., Williams, F.A. “Burning velocity of turbulent premixed flames in a high-pressure environment”, *Proc. Combust. Inst*. 26: 389-396 (1996).
[27] Bychkov, V., “Importance of the Darrieus-Landau instability for strongly corrugated turbulent flames”, *Phys. Rev. E* 68: 066304 (2003).
[28] Chaudhuri, S., Akkerman, V., Law, C.K., “Spectral formulation of turbulent flame speed with consideration of hydrodynamic instability”, *Phys. Rev. E* 84: 026322 (2011).
[29] Fogla, N., Creta, F., Matalon, M., “The turbulent flame speed for low-to-moderate turbulence intensities: Hydrodynamic theory vs. experiments”, *Combust. Flame* 175: 155-169 (2017).
[30] Yang, S., Saha, A., Liu, Z., Law, C.K., “Role of Darrieus-Landau instability in propagation of expanding turbulent flames”, *J. Fluid Mech*. 850: 784-802 (2018).
[31] Lapenna, P.E., Troiani, G., Lamioni, R., Creta, F., “Mitigation of Darrieus-Landau instability effects on turbulent premixed flames”, *Proc. Combust. Inst*. 38: 2885-2892 (2021).
[32] Chomiak, J., Lipatnikov, A.N., “A simple criterion of importance of laminar flame instabilities in premixed turbulent combustion of mixtures characterized by low Lewis numbers”, *Phys. Rev. E* 107: 015102 (2023).
[33] Frouzakis, C.E., Fogla, N., Tomboulides, A.G., Altantzis, C., Matalon, M., “Numerical study of unstable hydrogen/air flames: shape and propagation speed”, *Proc. Combust. Inst*. 35: 1087-1095 (2015).
[34] Berger, L., Attili, A., Pitsch, H., “Intrinsic instabilities in premixed hydrogen flames: Parametric variation of pressure, equivalence ratio, and temperature. Part 1 - Dispersion relations in the linear regime”, *Combust. Flame* 240: 111935 (2022).
[35] Liu, Z., Yang, S., Law, C.K., Saha, A., “Cellular instability in Le<1 turbulent expanding flames”, *Proc. Combust. Inst*. 37: 2611-2618 (2019).
[36] Day, M.S., Bell, J.B., Cheng, R.K., Tachibana, S., Beckner, V.E., Lijewski, M.J., “Cellular burning in lean premixed turbulent hydrogen-air flames: coupling experimental and computational analysis at the laboratory scale”, *J. Physics Conf. Series* 180: 012031 (2009).
[37] Howarth, T.L., Hunt, E.F., Aspden, A.J., “Thermodiffusively-unstable lean premixed hydrogen flames: Phenomenology, empirical modelling, and thermal leading points”, *Combust. Flame* 253: 112811 (2023).
[38] Day, M.S., Bell, J.B., Bremer, P.T., Pascucci, V., Beckner, V.E., Lijewski, M.J., “Turbulence effects on cellular burning structures in lean premixed hydrogen flames”, *Combust. Flame* 156: 1035-1045 (2009).
[39] Lee, H.C., Wu, B., Dai, P., Wan, M., Lipatnikov, A.N., “Turbulent burning velocity and thermodiffusive instability of premixed flames”, *Phys. Rev. E* 108: 035101 (2023).

[40] Lipatnikov, A.N., Lee, H.C., Wu, B., Dai, P., Wan, M., Sabelnikov, V.A., "Transition from turbulence-dominated to instability-dominated combustion regime in lean hydrogen-air flames", *Combust. Flame* 259: 113170 (2024).
[41] Sivashinsky, G.I., "Diffusional-thermal theory of cellular flames", *Combust. Sci. Technol*. 15: 137-146 (1977).
[42] Pelcé, P., Clavin, P., "Influence of hydrodynamics and diffusion upon the stability limits of laminar premixed flames", *J. Fluid Mech*. 124: 219-237 (1982).
[43] Matalon, M., Matkowsky, B.J., "Flames as gas dynamic discontinuities", *J. Fluid Mech*. 124: 239-260 (1982).
[44] Creta, F., Matalon, M., "Propagation of wrinkled turbulent flames in the context of hydrodynamic theory," *J. Fluid Mech*. 680: 225-264 (2011).
[45] Lee, H.C., Dai, P., Wan, M., Lipatnikov, A.N. "A DNS study of extreme and leading points in lean hydrogen-air turbulent flames - part I: Local thermochemical structure and reaction rates, *Combust. Flame* 235: 111712 (2022).
[46] Lee, H.C., Dai, P., Wan, M., Lipatnikov, A.N. "A DNS study of extreme and leading points in lean hydrogen-air turbulent flames - part II: Local velocity field and flame", *Combust. Flame* 235: 111716 (2022).
[47] Lee, H.C., Dai, P., Wan, M., Lipatnikov, A.N. "Influence of molecular transport on burning rate and conditioned species concentrations in highly turbulent premixed flames", *J. Fluid Mech*. 928: A5 (2021).
[48] Lee, H.C., Dai, P., Wan, M., Lipatnikov, A.N. "A numerical support of leading point concept", *Int. J. Hydrogen Energy*, 47: 23444-23461 (2022).
[49] Lee, H.C., Abdelsamie, A., Dai, P., Wan, M., Lipatnikov, A.N. "Influence of equivalence ratio on turbulent burning velocity and extreme fuel consumption rate in lean hydrogen-air turbulent flames", *Fuel* 327: 124969 (2022).
[50] Lee, H.C., Dai, P., Wan, M., Lipatnikov, A.N. "Displacement speed, flame surface density, and burning rate in highly turbulent premixed flames characterized by low Lewis numbers", *J. Fluid Mech*. 961: A21 (2023).
[51] Lee, H.C., Wu, B., Dai, P., Wan, M., Lipatnikov, A.N. "Area increase and stretch factor in lean hydrogen-air turbulent flames", *Proc. Combust. Inst*. 40: 105687 (2024).
[52] Kéromnès, A., Metcalfe, W.K., Heufer, K.A., Donohoe, N., Das, A.K., Sung, C.-J., Herzler, J., Naumann, C., Griebel, P., Mathieu, O., Krejci, M.C., Petersen, E.L., Pitz, W.J., Curran, H.J. "An experimental and detailed chemical kinetic modeling study of hydrogen and syngas mixture oxidation at elevated pressures", *Combust. Flame* 160: 995-1011 (2013).
[53] Goodwin, D., Malaya, N., Moffat, H., Speth, R., Cantera: An object-oriented software toolkit for chemical kinetics, thermodynamics, and transport processes, Caltech, Pasadena, CA, 2009.
[54] Abdelsamie, A., Fru, G., Oster, T., Dietzsch, F., Janiga, G., Thévenin, D., "Towards direct numerical simulations of low-Mach number turbulent reacting and two-phase flows using immersed boundaries", *Comput. Fluids* 131: 123-141 (2016).
[55] Bobbitt, B., Lapointe, S., Blanquart, G., "Vorticity transformation in high Karlovitz number premixed flames", *Phys. Fluids* 28: 015101 (2016).
[56] Landau, L.D., Lifshitz, E.M. *Fluid Mechanics*, Pergamon Press, 1987.
[57] Kadowaki, S., Hasegawa, T., "Numerical simulation of dynamics of premixed flames: flame instability and vortex-flame interaction", *Prog. Energy Combust. Sci*. 31: 193-241 (2005).
[58] Wen, X., Berger, L., Cai, L., Parente, A., Pitsch, H., "Thermodiffusively unstable laminar hydrogen flame in a sufficiently large 3D computational domain - Part I: Characteristic patterns", *Combust. Flame* 253: 112817 (2024).